Food & Function

ROYAL SOCIETY OF CHEMISTRY

PAPER

View Article Online
View Journal | View Issue

Cite this: *Food Funct.*, 2022, **13**, 10923

Isoquercitrin from *Apocynum venetum* L. produces an anti-obesity effect on obese mice by targeting C-1-tetrahydrofolate synthase, carbonyl reductase, and glutathione *S*-transferase P and modification of the AMPK/SREBP-1c/FAS/CD36 signaling pathway in mice *in vivo*†

Majid Manzoor, [a] Makoto Muroi, [b] Naoko Ogawa,[b] Hiroki Kobayashi,[c] Haruna Nishimura,[c] Danni Chen, [a] Opeyemi B. Fasina, [a] Jianyu Wang, [a] Hiroyuki Osada, [b] Minoru Yoshida, [c,d] Lan Xiang *[a] and Jianhua Qi *[a]

In the present study, mice with high-fat-diet-induced obesity were used in investigating the anti-obesity effects of an aqueous extract and isoquercitrin from *Apocynum venetum* L. The aqueous extract and the signal molecule isoquercitrin significantly reduced the body weight gain, food intake, water consumption, and fasting blood glucose, plasma triglyceride and total cholesterol levels of the obese mice. Furthermore, the mechanism of action of isoquercitrin was explored through RT-PCR analyses and uptake experiments of adenosine 5′-monophosphate-activated protein kinase (AMPK) and sterol regulatory-element binding protein (SREBP-1c) inhibitors and glucose. The indexes of SREBP-1c, fatty acid synthase (FAS), stearoyl-CoA desaturase-1 (SCD), and cluster of differentiation 36 (CD36) in obese mice significantly increased but returned to normal levels after the administration of isoquercitrin. Meanwhile, the anti-obesity effect of isoquercitrin was diminished by the inhibitors of AMPK and SREBP-1c. In addition, intestinal glucose uptake in normal mice was significantly inhibited after the oral administration of isoquercitrin. Moreover, 2D gel electrophoresis based proteome-wide cellular thermal shift assay (CETSA) showed that the potential target proteins of isoquercitrin were C-1-tetrahydrofolate synthase, carbonyl reductase, and glutathione *S*-transferase P. These results suggested that isoquercitrin produces an anti-obesity effect by targeting the above-mentioned proteins and regulating the AMPK/SREBP-1c signaling pathway and potentially prevents obesity and obesity-related metabolic disorders.

Received 18th August 2022,
Accepted 28th September 2022

DOI: 10.1039/d2fo02438a

rsc.li/food-function

1. Introduction

Affecting approximately one-third of the global population, obesity is an alarming medical condition. In particular, the global rise in obesity prevalence is attributed to urbanization. The WHO reported that more than two billion people are overweight, and more than 650 million people are obese worldwide.[1] Since 1980, the number of obese people has doubled in more than 70 nations.[2] More seriously, obesity not only leads to metabolic syndrome[3] but also increases the risk of cardiovascular morbidity, cancer,[4] and cognitive dysfunctions,[5] which affects the health condition of human beings and increases the socio-economic burden. However, commercial anti-obesity drugs have certain limitations due to drug withdrawal symptoms and adverse effects that require additional therapeutic interventions.[6] In this regard, nutrient-dense diets and functional food in the form of extracts or active molecules can be considered novel treatment options to overcome obesity.

Obesity is the result of energy metabolism dysfunction in organisms. In energy metabolism, the adenosine 5′-monophosphate (AMP)-activated protein kinase (AMPK) signaling

[a]*College of Pharmaceutical Sciences, Zhejiang University, 866 Yu Hang Tang Road, Hangzhou, P. R. China. E-mail: lxiang@zju.edu.cn, qijianhua@zju.edu.cn; Fax: +86-571-8826-8627; Tel: +86-571-8826-8627*
[b]*Chemical Biology Research Group, RIKEN Center for Sustainable Resource Science, Wako-shi, Saitama 351-0198, Japan*
[c]*Chemical Genomics Research Group, RIKEN Center for Sustainable Resource Science, 2-1 Hirosawa, Wako, Saitama 351-0198, Japan*
[d]*Department of Biotechnology and Collaborative Research Institute for Innovative Microbiology, The University of Tokyo, Yayoi 1-1-1, Bunkyo-ku, Tokyo 113-8657, Japan*

†Electronic supplementary information (ESI) available. See DOI: https://doi.org/10.1039/d2fo02438a

pathway plays an important role. AMPK is an AMP-dependent protein kinase and a key molecule in the regulation of bioenergy metabolism and the core of the study of diabetes and other metabolism-related diseases. It is expressed in various organs related to metabolism and can be activated by various stimuli in the body, including cell pressure, exercise, hormones, and substances that can affect cell metabolism. Its activation can alleviate metabolic imbalance caused by type II diabetes.[7] AMPK activity is regulated through phosphorylation regulated by its energy-sensing domains. Characteristically, different metabolic states lead to shifts in the AMP : ATP ratio and glycogen-induced changes in cellular energy homeostasis, and the lipid and NAD/NADH balance regulates the AMPK activity.[8] Nevertheless, distinct pathways may be responsible for AMPK regulation independent of the energy states in cells. Metformin can phosphorylate and activate AMPK without changing the energy states in cells.[9] Leptin-stimulated AMPK activation can be either AMP dependent or AMP independent.[10]

Sterol regulatory element binding proteins (SREBPs) are transcription factors that mediate fatty acid synthesis, cholesterol homeostasis, lipogenesis, and adipogenesis.[11] Stearoyl-CoA desaturase-1 (SCD) is the key protein expressed in the adipose tissues of organisms and selectively mediates lipogenesis by regulating fatty acid and triglyceride synthesis.[12] AMPK is an upstream regulator of SREBP-1c, and AMPK activity negatively correlates with SREBP-1c activity in the liver and hepatocytes.[13] Hence, AMPK activation represses SREBP-1c activity, and the subsequent activation of catabolic pathways and inhibition of anabolic pathways ultimately inhibit fatty acid synthesis and lipogenesis. Conversely, AMPK inhibition increases the expression of SREBP-1c and promotes fatty acid synthesis and lipogenesis. Reduction in AMPK expression and increase in SREBP-1c expression have been reported in high-fat diet (HFD)-fed obese mice.[14,15] Therefore, we focused on these signaling pathways to clarify the action mechanism of isoquercitrin in the present study.

Apocynum venetum, a member of the oleander family, has 3 species named *Apocynum venetum* L., *Poacynum pictum* (Sckrenk) Baill and *Poacynum hendersonii* (Hook.f) Woodson.[16] In Xinjiang (China), herbal tea from *Apocynum venetum* L. (AV) is prepared by processing its leaves that generate a unique flavor and taste through fermentation after drying. The raw leaves mainly contain glycosides, flavonols, tannic acid and its derivatives, triglycerides, sterols, aliphatic organic compounds and amino acids; therefore, the numerous medicinal uses of AV as an anti-depressant, anti-hypertensive, anti-hyperlipidemic, anti-aging, antibacterial, and immunity-enhancing agent might be attributed to these chemical constituents.[17–19] AV leaves are rich in flavonol glycosides and flavonols as major active medicinal ingredients.[16] Isoquercitrin is one of the most abundant flavonol glycosides in AV leaves, exhibiting antioxidant, anti-inflammatory, anticancer, and antidiabetic activities.[20–22] However, the anti-obesity effect and action mechanism of this compound remain unclear. In the present study, we used HFD-induced obese mice, which are considered suitable models for investigating dietary obesity, to investigate the anti-obesity effect of an aqueous AV extract and purified isoquercitrin. Furthermore, we used isoquercitrin to analyze the mechanism of action. We found that isoquercitrin exerted its anti-obesity effect on HFD-fed obese mice by targeting C-1-tetrahydrofolate synthase, carbonyl reductase, and glutathione *S*-transferase P and modifying the AMPK/SREBP-1c/fatty acid synthase (FAS)/cluster of differentiation 36 (CD36) signaling pathway *in vivo*.

2. Results

2.1. *A. venetum* L. aqueous extract prevents HFD-induced obesity in mice *in vivo*

First, we observed variations in the body weight gain, food intake, and water consumption of mice after treatment with the aqueous extract of AV. We found that the HFD control group maintained higher body weight gain and food intake than the ND group (Fig. 1B and C, $p < 0.001$) but had a lower water consumption rate (Fig. 1D, $p < 0.001$). Nonetheless, in the treatment groups, which received HFD and AV aqueous extracts at doses of 5 and 50 mg kg^{-1}, significant decreases in body weight gain (Fig. 1B), food intake (Fig. 1C), and water consumption (Fig. 1D) were observed compared to those in the HFD control group ($p < 0.05$, $p < 0.01$, and $p < 0.001$). Second, we sacrificed the mice and collected their plasma samples for biochemical analysis after 1 month of trial. Blood glucose levels were significantly lower in all the treatment groups than the blood glucose level of the HFD control group (Fig. 1E, $p < 0.001$). Similarly, obese mice in the treatment groups showed significantly lowered levels of TG, TC, LDL-C, and HDL-C, compared with the HFD control group (Fig. 1E, $p < 0.05$, $p < 0.01$, $p < 0.01$, and $p < 0.001$). These differences were consistent with the differences between the HFD control and ND control groups. Moreover, the weights of the livers of obese mice in the AV aqueous extract-treated group were significantly lower at all doses of the AV aqueous extract. However, epididymal fat weight was significantly lower only for the 5 mg kg^{-1} dose when compared to the HFD group (Fig. 1F, $p < 0.001$). Altogether, these results indicate that the AV aqueous extract prevents HFD induced obesity and 5 mg kg^{-1} is the best concentration.

2.2. Isoquercitrin reduces HFD-induced obesity and obesity parameters of mouse

We separated the active AV aqueous extract to purify isoquercitrin and conducted an anti-obesity animal trial. Using the mouse model of obesity, we supplemented the obese mice with isoquercitrin at doses of 0.1, 0.5, and 5 mg kg^{-1}, the AV aqueous extract at a dose of 5 mg kg^{-1}, and metformin at a dose of 140 mg kg^{-1} as the positive control. We found that isoquercitrin reduced body weight gain in a dose-dependent manner in the HFD-fed obese mice (Fig. 2A, $p < 0.05$, $p < 0.01$, and $p < 0.001$), and these effects were consistent with those in the groups treated with the AV aqueous extract (Fig. 2A,

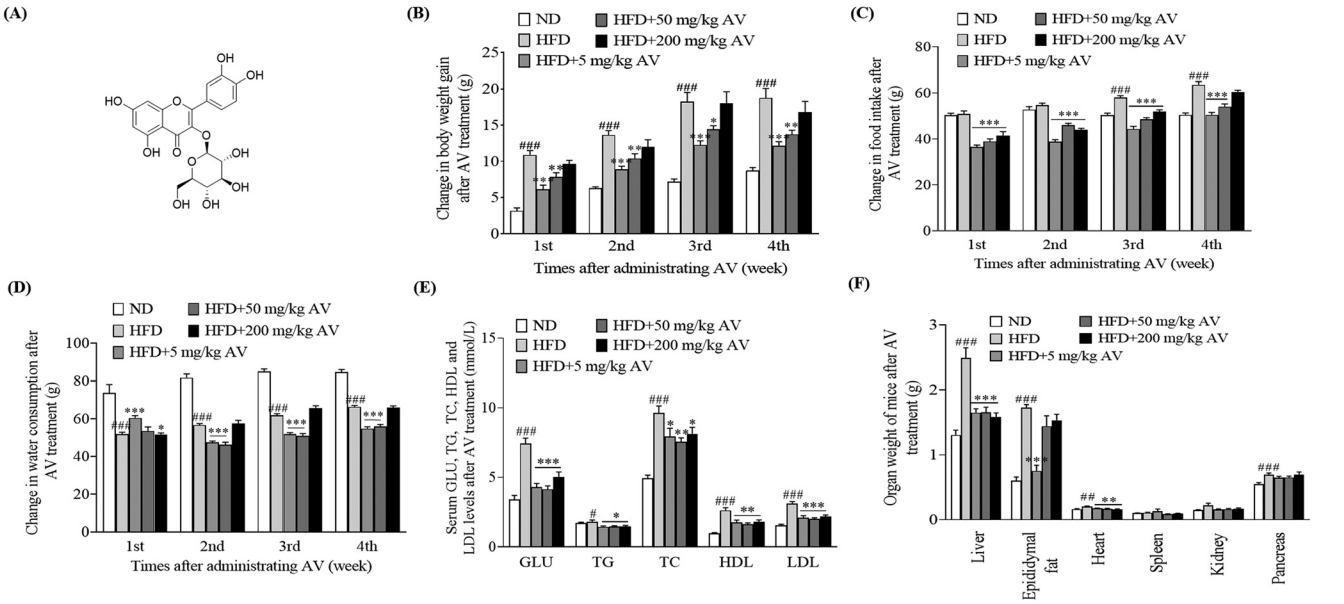

Fig. 1 The chemical structure of isoquercitrin and the anti-obesity effects of the AV aq. extract on HFD-induced obese mice. (A) Chemical structure of isoquercitrin and changes in (B) body weight, (C) food intake, (D) water consumption, (E) serum GLU, TG, TC, HDL and LDL levels and (F) organ weight of obese mice after administering the AV aq. extract at doses of 5, 50 and 200 mg kg^{-1} for four weeks. Data are represented as the mean ± SEM at the corresponding time intervals. Each group has ten mice, and the experiment was performed in triplicate. $^{\#}$, $^{\#\#}$ and $^{\#\#\#}$ correspond to the significant differences when compared with the normal control at $p < 0.05$, $p < 0.01$, and $p < 0.001$. *, ** and *** point to the significant differences in comparison with the HFD group at $p < 0.05$, $p < 0.01$ and $p < 0.001$.

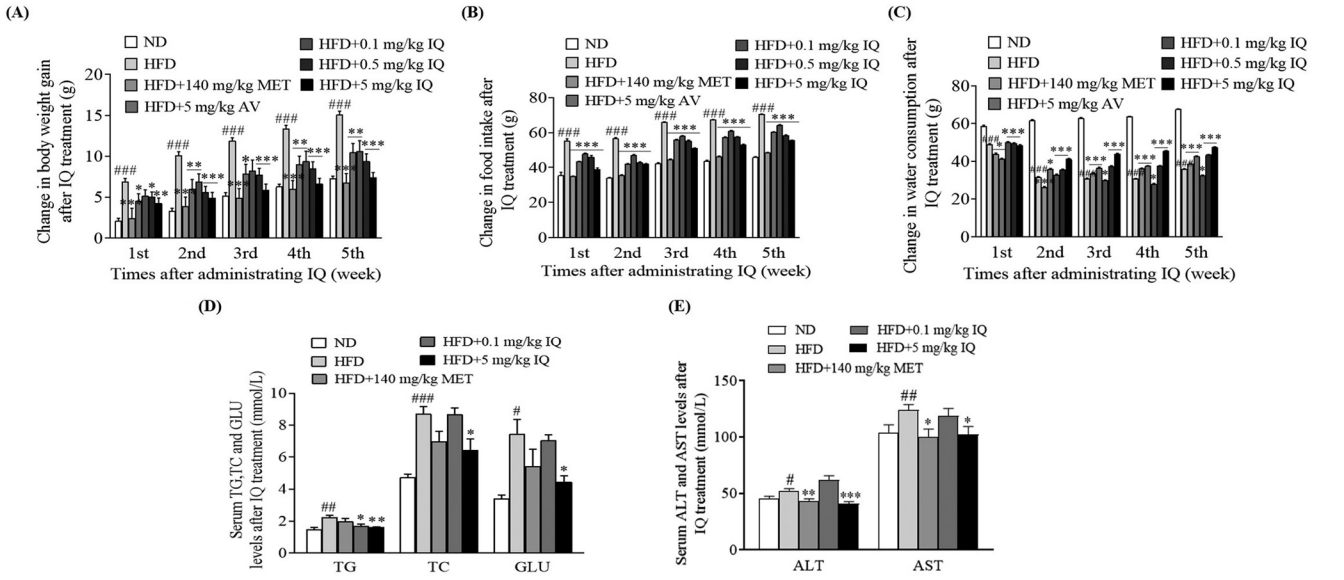

Fig. 2 Anti-obesity effects of isoquercitrin on HFD-induced obese mice. The changes in (A) body weight gain, (B) food intake, (C) water consumption, (D) serum TG, TC, and GLU levels, and (E) ALT and AST enzyme levels in obese mice after administering isoquercitrin for five weeks. Data are represented as the mean ± SEM at the corresponding time points. The number of mice per group is eight, and the experiment is repeated three times. $^{\#}$, $^{\#\#}$, and $^{\#\#\#}$ represent the significant differences in comparison with the normal control at $p < 0.05$, $p < 0.01$, and $p < 0.001$. *, ** and *** indicate the significant differences in comparison with the HFD group at $p < 0.05$, $p < 0.01$ and $p < 0.001$.

$p < 0.01$) and metformin (Fig. 2A, $p < 0.001$). Correspondingly, isoquercitrin supplementation significantly reduced the food intake of the obese mice in a dose-dependent manner compared with that of the HFD control group (Fig. 2B, $p < 0.001$), suggesting that isoquercitrin reduced obesity and obesity parameters partly due to reduced food intake. However, water consumption in the isoquercitrin- and metformin-treated groups was significantly higher than that in the HFD control group

(Fig. 2C, $p < 0.001$ and $p < 0.01$). Obesity is regarded as a risk factor for dyslipidemia, which is characterized by increased TG and TC levels. Hence, we also evaluated the blood biochemical parameters in the HFD control and isoquercitrin-treated groups (ESI Table 1†). Isoquercitrin at a dose of 5 mg kg^{-1} significantly reduced the plasma TG and TC levels of obese mice compared with those in the HFD control group (Fig. 2D, $p < 0.01$ and $p < 0.05$). These reductions were comparable with those in the ND and metformin-treated groups (Fig. 2D). In obese individuals, no explicit symptoms were observed even though the liver enzyme levels were elevated and the disease advanced up to hepatic failure. Therefore, asymptomatic individuals with mildly elevated liver enzyme levels (ALT and AST) presented risks of liver diseases, mainly nonalcoholic fatty liver disease and hepatitis. In this regard, we demonstrated that the plasma levels of ALT and AST were reduced significantly after 5 mg kg^{-1} isoquercitrin treatment in comparison with those of the HFD control group (Fig. 2E, $p < 0.001$ and $p < 0.05$). These results indicated that isoquercitrin exerted an anti-obesity effect on the obese mice and it is the main active molecule of *A. venetum* L.

2.3. Isoquercitrin eliminates fatty liver and reduces epididymal fat tissues

Liver weight correlates positively with body weight gain and obesity, and fat accumulation in the liver leads to fatty liver disease. Fatty liver results in liver injury, scar tissue, and finally liver function abnormalities. The marked changes in liver weight due to HFD-induced obesity are displayed in Fig. 3 and ESI Table 2.† Liver weight significantly increased in the HFD control group in comparison with that in the ND control group (Fig. 3A, $p < 0.001$). The reversal of increased liver weight was statistically significant after isoquercitrin treatment in obese mice at 0.5 and 5 mg kg^{-1} doses (Fig. 3A, $p < 0.001$ and $p < 0.001$). A similar trend of decreased liver weight was observed in the groups treated with the AV aqueous extract and metformin (Fig. 3A, $p < 0.01$ and $p < 0.01$). Visceral adipose tissues show a higher lipolytic tendency, thus providing a major supply of free fatty acids and contributing to obesity-related comorbidities.[23] Therefore, epididymal fat tissues were weighed, and differences between the HFD and ND control groups were observed. A significant increase in the weight of epididymal fat tissues was observed in the HFD control group (Fig. 3B, ESI Table 2,† $p < 0.001$). However, isoquercitrin treatment at doses of 0.5 and 5 mg kg^{-1} significantly reduced epididymal fat tissue weight compared to that in the HFD control group (Fig. 3B, $p < 0.01$ and $p < 0.01$). AMPK has a pivotal role in hepatic metabolism and maintains balanced levels of fats and lipids in the body. As the AMPK activation is evaluated by its phosphorylation,[13] we measured AMPK activation in liver tissues. Our experimental results indicated that the relative protein expression of P-AMPK/AMPK was significantly reduced in the livers of obese mice compared to that in control mice (Fig. 3C, ESI Fig. 1,† $p < 0.05$); however, the relative expression of P-AMPK/AMPK was significantly increased in the 5 mg kg^{-1} isoquercitrin treated group (Fig. 3C, ESI Fig. 1,† $p < 0.05$) when

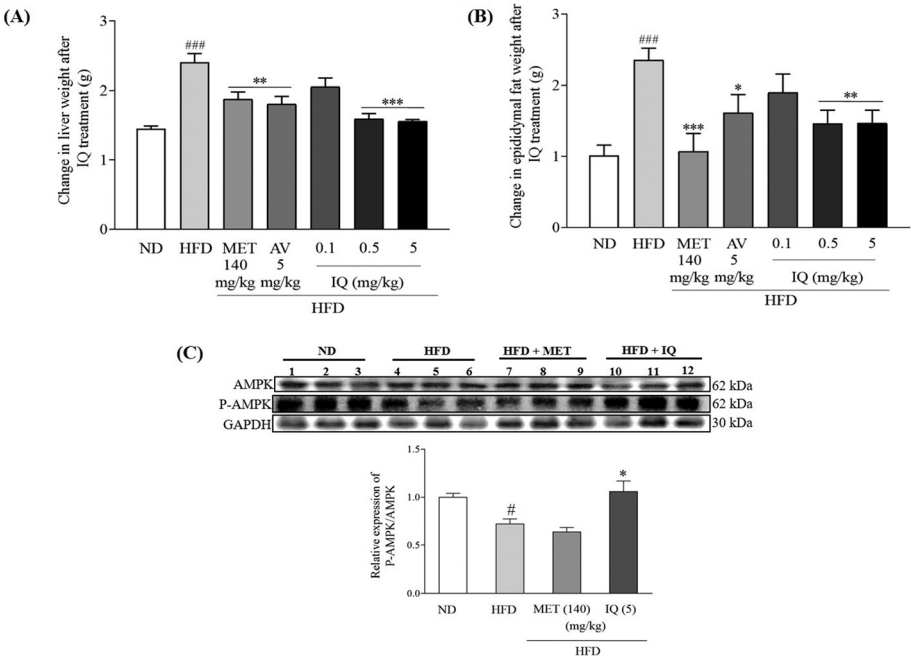

Fig. 3 Effects of isoquercitrin on the liver and adipose tissues of obese mice and AMPK activation. The changes in the (A) weight of the liver, (B) epididymal fat weight and (C) relative protein expression of P-AMPK/AMPK in the liver of obese mice after isoquercitrin treatment. Shown are the mean ± SEM and 8 mice are present in each group. #, ## and ### represent the significant differences in comparison with the normal control at $p < 0.05$, $p < 0.01$, and $p < 0.001$. *, ** and *** represent the significant differences in comparison with the HFD group at $p < 0.05$, $p < 0.01$ and $p < 0.001$ as indicated.

compared to the HFD control group. Overall, these results implied that isoquercitrin reduced fatty liver and lessened visceral fat burden in HFD-induced obese mice through the activation of AMPK.

2.4. Isoquercitrin inhibits gene expression-related adipogenesis and TG and TC accumulation in the liver and the inhibitor of SREBP-1c removes the anti-obesity effect of isoquercitrin

The molecular mechanism was examined, and the liver tissues of mice were analyzed to examine the mRNA expression of the lipogenic transcription factor SREBP-1c, and adipogenesis genes, such as FAS, SCD-1, and CD36. The HFD control group showed significantly increased mRNA expression levels of SREBP-1c, FAS, SCD-1, and CD36 genes in the liver tissues compared with the ND control group (Fig. 4A, $p < 0.001$, $p < 0.01$, $p < 0.001$ and $p < 0.001$). Concurrently, the mRNA expression of the same genes showed a significant decline after supplementation with isoquercitrin at a dose of 5 mg kg^{-1} (Fig. 4A, $p < 0.01$, $p < 0.01$, $p < 0.01$ and $p < 0.01$) compared with that in the HFD control group. Furthermore, we used the competitive inhibitor of SREBP site 1 protease (PF429242) to evaluate the effects of SREBP-1c inhibition on body weight gain, food intake, and water consumption *in vivo*. A significant decrease in body weight gain was observed when 5 mg kg^{-1} isoquercitrin was administered alone in obese mice compared with the body weight gain in the HFD control group (Fig. 4B, $p < 0.05$ and $p < 0.001$). However, the concomitant administration of 5 mg kg^{-1} isoquercitrin and 2.5 mg kg^{-1} PF429242 in obese mice did not show a significant effect on body weight gain (Fig. 4B). Likewise, food intake and water consumption in the isoquercitrin-treated group significantly decreased (Fig. 4C and D, $p < 0.001$, $p < 0.001$ and $p < 0.01$), whereas no significant differences in food intake and water consumption were observed in the group that received isoquercitrin and PF429242 compared with the HFD control group (Fig. 4C and D). Moreover, the effects of isoquercitrin on the liver and epididymal adipose tissue of obese mice were diminished by PF429242 (ESI Table 3†). Excessive amounts of free fatty acids from the HFD fluxed into the liver tissues for lipogenesis and accumulated in the liver in the form of oil droplets.[24] Therefore, we measured the hepatic lipid levels of TG and TC in the mice after administration of isoquercitrin alone and after simultaneous administration of isoquercitrin and PF429242. The HFD control group showed significantly higher TG levels than the ND control group (Fig. 4E, $p < 0.01$), and a prominent decline was observed in hepatic TG levels after isoquercitrin supplementation (Fig. 4E, $p < 0.05$). However, in the group that received isoquercitrin and PF429242, the TG levels in the liver tissues were comparable to those in the HFD control group, and no significant difference was observed due to SREBP-1c inhibition (Fig. 4E). Similar results were observed for hepatic TC levels. A significant decrease in the hepatic TC level was noted after isoquercitrin treatment (Fig. 4F, $p < 0.01$). Nevertheless, this effect was diminished in the presence of PF429242. These results demonstrated that isoquercitrin regu-

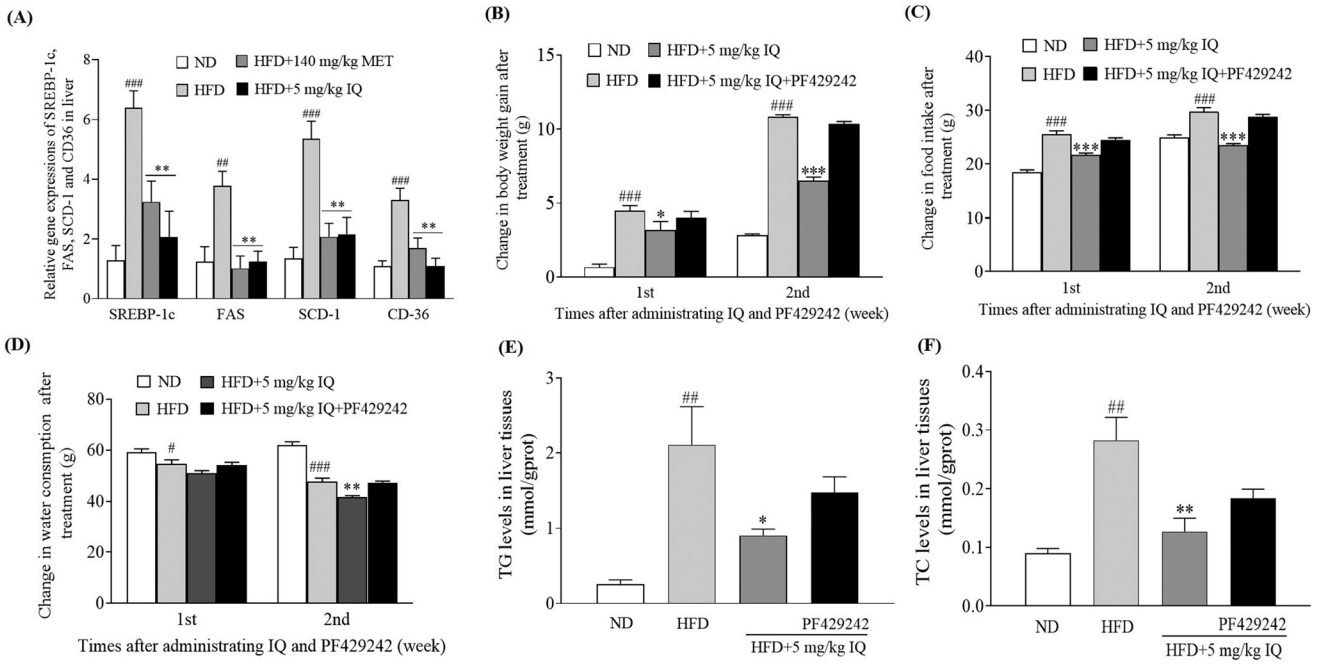

Fig. 4 Effects of isoquercitrin on SREBP-1c related adipogenesis and hepatic lipid accumulation. (A) Gene expressions of SREBP-1c, SCD-1, FAS, and CD36, and the effect of the SREBP-1c inhibitor on (B) body weight gain, (C) food intake, (D) water consumption, and hepatic (E) TG and (F) TC levels of obese mice. Data represent the mean ± SEM and the number of mice in each group is 6. $^{\#}$, $^{\#\#}$, and $^{\#\#\#}$ represent the significant differences when comparing the normal control with the HFD group at $p < 0.05$, $p < 0.01$, and $p < 0.001$. *, ** and *** indicate the significant differences when comparing the treatment groups with the HFD group at $p < 0.05$, $p < 0.01$ and $p < 0.001$.

lated adipogenesis by modulating SREBP-1c in the liver of obese mice.

2.5. Inhibitor of AMPK diminishes the anti-obesity effects of isoquercitrin in mice *in vivo*

AMPK activation leads to Ser372 phosphorylation, which represses SREBP-1c-related gene expression by limiting its cleavage and nuclear translocation and consequently leads to reduced lipid buildup and lipogenesis.[13] Therefore, after confirming the SREBP-1c-related gene expression changes due to isoquercitrin treatment, we used one AMPK inhibitor, compound C, to block AMPK activity *in vivo* and evaluated whether the AMPK/SREBP-1c signaling pathway is involved in the anti-obesity effects of isoquercitrin. The alterations in body weight gain, food intake, water consumption, and liver and epididymal fat weights after AMPK inhibition are displayed in Fig. 5A–E and ESI Table 3.† The body weight gain of obese mice was significantly higher than that of ND control mice, and this weight gain was reversed predominantly in obese mice after isoquercitrin supplementation (Fig. 5A, $p < 0.05$ and $p < 0.01$). However, the anti-obesity effects of isoquercitrin on obese mice that received isoquercitrin and the AMPK inhibitor diminished due to the inhibition of AMPK (Fig. 5A). Additionally, food intake was reduced significantly in isoquercitrin-administered obese mice, and the intake rate was not altered significantly after AMPK inhibition compared with that in the HFD control group (Fig. 5B, $p < 0.05$). Water consumption did not significantly change in the isoquercitrin- and AMPK-inhibitor-treated groups compared with the HFD control group (Fig. 5C). Moreover, we weighed the liver and epididymal fat after sacrificing the mice. We observed that the liver and epididymal fat weighed significantly lower in the isoquercitrin-treated group than those in the HFD control obese mice (Fig. 5D and E, ESI Table 3,† $p < 0.001$ and $p < 0.001$). However, the liver and epididymal fat weights were comparable to those in the HFD control group and did not differ significantly in the AMPK-inhibited group (Fig. 5D and E, ESI Table 3†). These results illustrated that isoquercitrin regulated SREBP-1c-related adipogenesis through AMPK *in vivo*.

2.6. Isoquercitrin inhibits intestinal glucose uptake in mice *via* reduction of GLUT2 levels in the intestine and liver

Glucose is mainly absorbed through intestinal epithelial cells. Excessive glucose absorption through the intestine is the primary reason for fat accumulation and obesity.[25] In addition, the excessive intestinal absorption of glucose may interfere with the absorption of other essential nutrients and leads to nutritional imbalance. To determine whether isoquercitrin affects glucose uptake in the intestine of mice, we performed an oral glucose tolerance test *in vivo*. First, we administered glucose and isoquercitrin simultaneously and measured the blood glucose concentration every 20 min. Isoquercitrin significantly decreased the blood glucose concentration from 80 min to 120 min compared with the concentration in the control group (Fig. 6A, $p < 0.01$, $p < 0.01$, and $p < 0.01$). Next, we administered isoquercitrin to the mice and subsequently performed glucose treatment after 10 min. The glucose concentration was significantly reduced by isoquercitrin (Fig. 6B,

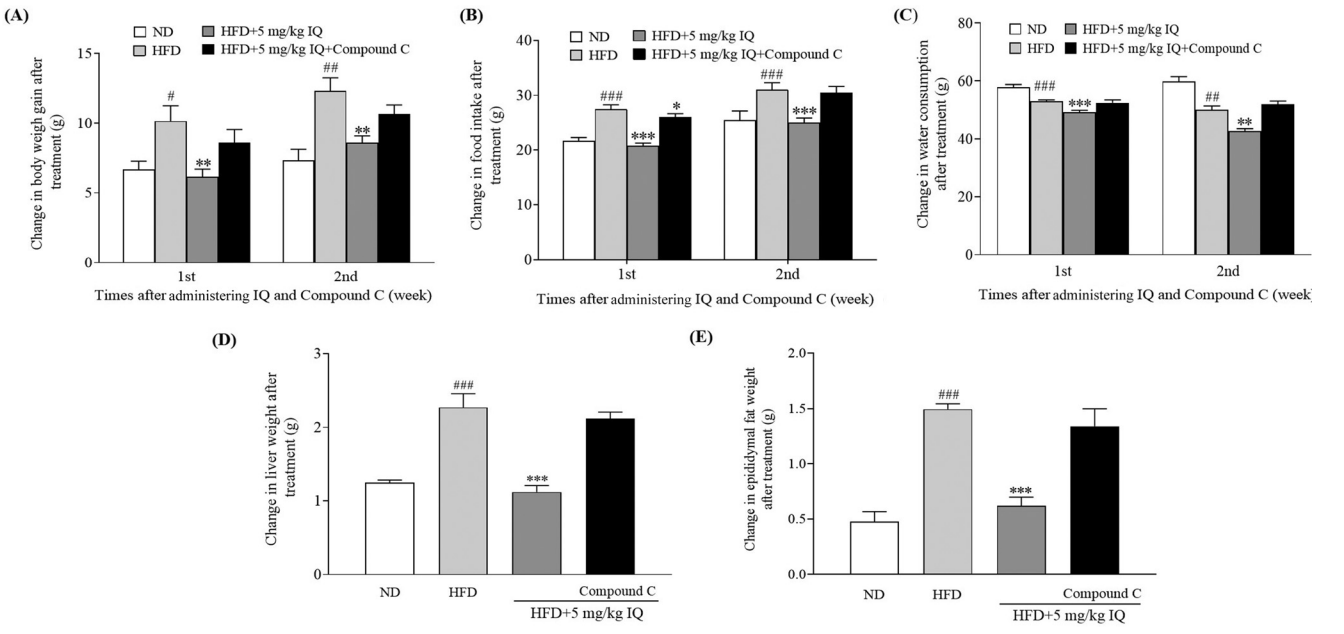

Fig. 5 Effect of the AMPK inhibitor on the anti-obesity effects of isoquercitrin. The changes in (A) body weight gain, (B) food intake, (C) water consumption, and (D) liver and (E) epididymal fat weight of obese mice. The number of mice in each group is 6 and the values represent the mean ± SEM. #, ##, and ### represent the significant differences when comparing the normal control with the HFD group at $p < 0.05$, $p < 0.01$, and $p < 0.001$. ** and *** indicate the significant differences when comparing the treatment groups with the HFD group at $p < 0.01$ and $p < 0.001$ as indicated.

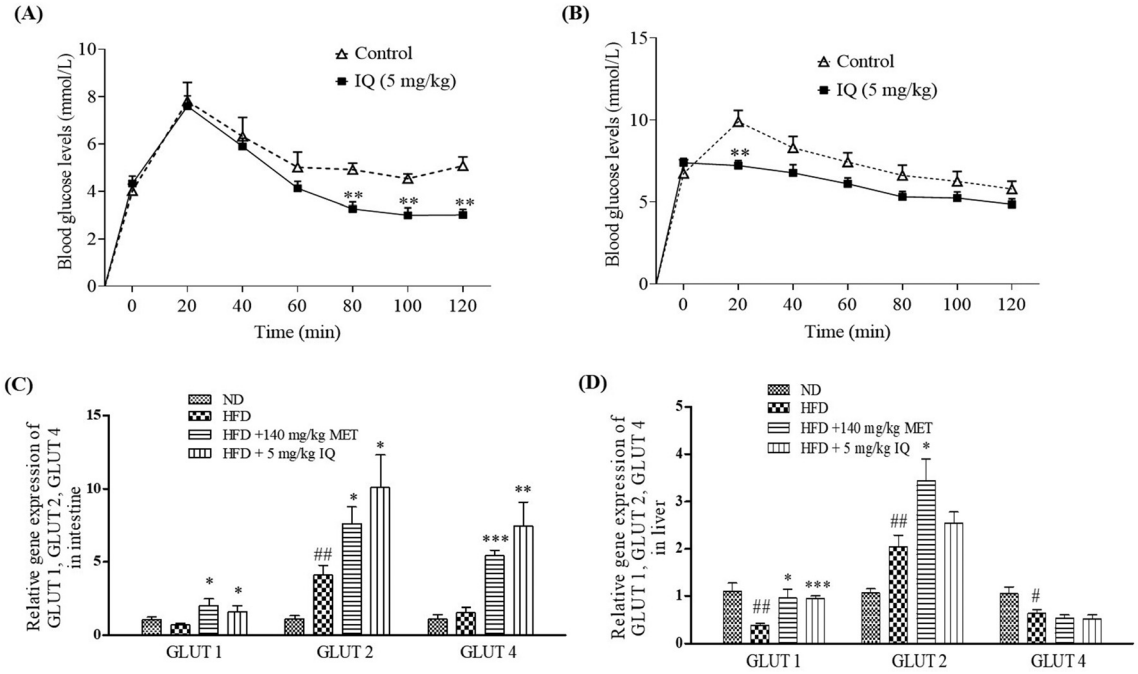

Fig. 6 Effect of isoquercitrin on intestinal glucose uptake in fasted mice and *GLUT* gene expression in obese mice. The changes in blood glucose of fasted mice after (A) oral co-administration of isoquercitrin and glucose and (B) pretreatment with isoquercitrin prior to glucose oral administration. (C and D) *GLUT1, GLUT2* and *GLUT4* gene expression in the intestine and liver, respectively. The number of mice in each group is 7 and the values represent the mean ± SEM. ** indicates the significant differences when comparing the treatment group with the control group at $p < 0.01$ in (A) and (B). # and ## indicate significant differences compared with the control group at $p < 0.05$ and $p < 0.01$ in (C) and (D). *, ** and *** represent significant differences compared with the HFD control group at $p < 0.05$, $p < 0.01$ and $p < 0.001$ in (C) and (D).

$p < 0.01$). Furthermore, we investigated the gene expression levels of glucose transporters, such as *GLUT1*, *GLUT2* and *GLUT4*, in the intestines and livers of obese mice after administering isoquercitrin. The gene expression levels of *GLUT1* and *GLUT4* in the intestine did not significantly change in the obese mice. By contrast, *GLUT2* gene expression significantly increased compared with that in the normal control (Fig. 6C, $p < 0.01$). After isoquercitrin treatment, *GLUT1*, *GLUT2*, and *GLUT4* gene expression in the intestines of the obese mice significantly increased (Fig. 6C, $p < 0.05$, $p < 0.05$ and $p < 0.01$). The gene expression levels of *GLUT1* and *GLUT4* in the livers of the obese mice significantly decreased, whereas the *GLUT2* gene expression in the liver was obviously increased compared with that of the normal control (Fig. 6D, $p < 0.01$, $p < 0.05$, and $p < 0.05$). Meanwhile, only *GLUT1* gene expression was significantly increased by isoquercitrin in the livers of the obese mice (Fig. 6D, $p < 0.001$). These results suggested that the compound inhibited the intestinal glucose uptake in mice and decreased the blood glucose levels of the obese mice by regulating *GLUT* gene expression in the intestine and liver.

2.7. Isoquercitrin did not affect the oxygen consumption rate and reduced extracellular acidification rate in HeLa cells

We used an extracellular flux analyzer to determine whether isoquercitrin affects the balance of glycolytic flux and mitochondrial respiration in HeLa cells. The oxygen consumption rate (OCR) was not affected by isoquercitrin (Fig. 7A). However, the external cellular acidification rate (ECAR) decreased after treatment with 10 μg mL^{-1} isoquercitrin (Fig. 7B). These results indicated that isoquercitrin mainly affected the glycolytic pathway and energy metabolism.

2.8. Isoquercitrin may target C-1-tetrahydrofolate synthase, protein gamma lutamyltransferase E, aldo-keto reductase family 1 member B1, carbonyl reductase, proteasome activator complex subunit 3, and glutathione *S*-transferase P in HeLa cells

To determine which proteins are the targets of isoquercitrin, we investigated the thermal stability-shifted proteins treated with isoquercitrin by using the 2DE-CETSA. After treatment with DMSO or isoquercitrin and heating at 40 °C, 45 °C, 50 °C and 55 °C, proteins in the cell lysates of HeLa cells were labeled with different fluorescent dyes (Cy3 or Cy5) and subjected to 2-D DIGE analysis. After the quantification of each spot, melting curves of 693 spots reproducibly detected in all gels were drawn. Among them six positive spots were observed at 101, 76.7, 40.4, 30.3, 30.8, and 23.3 kDa, which indicated thermal stabilization or destabilization upon isoquercitrin treatment (Fig. 8A). These spots were excised and identified as C-1-tetrahydrofolate synthase (no. 258), carbonyl reductase (NADPH) 1 (no. 957), phosphoglycerate kinase 1, glutathione *S*-transferase P (no. 1108), protein-glutamine gamma-glutamyltransferase E (no. 765), and aldo-keto reductase family 1 member B1 (890) by LC-MS/MS (Fig. 8B). These results indi-

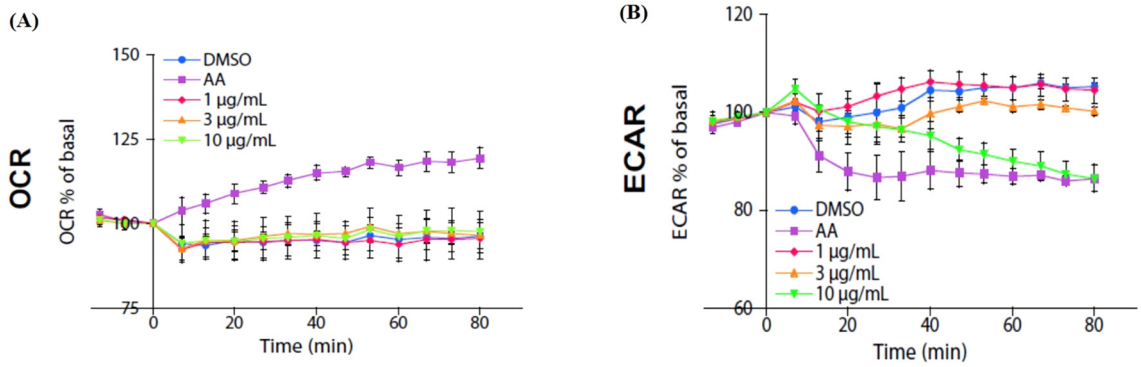

Fig. 7 Effect of isoquercitrin on the oxygen consumption rate and extracellular acidification rate in HeLa cells. The changes in the oxygen consumption rate (A) and extracellular acidification rate (B) in HeLa cells after treating with isoquercitrin at different doses of 1, 3, and 10 μg mL^{-1}. AA represents A76662 and AICAR.

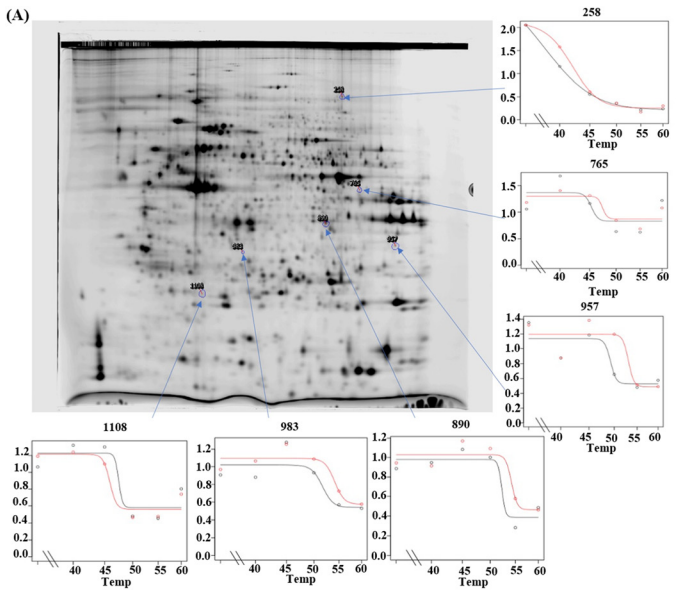

(B)

Estimated spots

Compound	SPOT No.	Score	emPAI	MW	GI	Protein name
Isoquercitrin	258	3251	3.92	101495	gil115206	C-1-tetrahydrofolate synthase, cytoplasma
	765	569	0.55	76710	gil80478896	Protein-glutamine gamma-glutamyltransferase E
	890	746	2.52	35830	gil4502049	Aldo-keto reductase family 1 member B1
	957	494	1.97	30356	gil4502599	Carbonyl reductase [NADPH] 1
	983	528	1.64	30866	gil531167	Proteasome activator complex subunit 3
	1108	693	2.58	23335	gil5822569	Glutathione S-transferase P

Fig. 8 Pre-identification of the target proteins for isoquercitrin in HeLa cells. (A) The result of 2DE-CETSA of HeLa cells after treatment with isoquercitrin at different temperatures. (B) The result of LC-MS/MS analysis for the spots in (A).

cated that these proteins are the potential target proteins of isoquercitrin in HeLa cells.

2.9. Isoquercitrin targets C-1-tetrahydrofolate synthase, carbonyl reductase, proteasome activator complex subunit 3, and glutathione *S*-transferase P in the livers of mice

To understand whether these proteins are the potential target proteins of isoquercitrin in mice, we treated mice with 5 mg kg^{-1} isoquercitrin for 1 week. The livers of the mice in the isoquercitrin-treated and control groups were collected. We used specific antibodies for western blotting analysis after heating at different temperatures such as 40 °C, 45 °C, 50 °C and 55 °C. The results are shown in Fig. 9. Interestingly, reductions in the protein levels of C-1-tetrahydrofolate synthase and carbonyl reductase were observed in the isoquercitrin-treated group (Fig. 9A and B, ESI Fig. 1 and 2†). Meanwhile, only the protein level of glutathione *S*-transferase P in the isoquercitrin-treated group significantly increased compared with that in the control group (Fig. 9C, ESI Fig. 1 and 2†). These results suggested that these enzymes are the potential target proteins of isoquercitrin to produce an anti-obesity effect on obese mice.

3. Discussion

Obesity, a leading cause of hypertension, heart diseases, and metabolic syndrome, is an alarming global health problem. Functional food and ingredients can exert anti-obesity effects.[26] *Apocynum venetum* L. (Luobuma) is one of the drug-homologous food plants in China. It is usually used as traditional Chinese tea, and the hepatoprotective, cardiotonic,

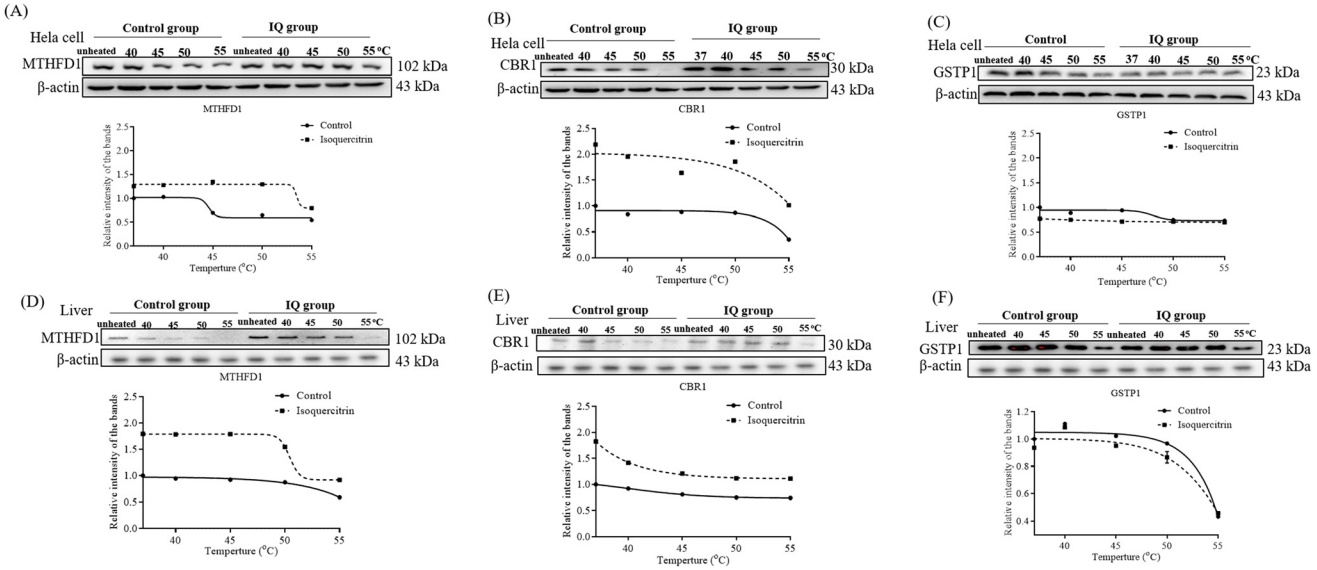

Fig. 9 The identification of the target proteins for isoquercitrin in HeLa cells and mouse livers. The changes in the proteins MTHFD1 (A), CBR1 (B) and GSTP1 (C) in HeLa cells after administering isoquercitrin and heating the samples at different temperatures, respectively. The changes in the proteins MTHFD1 (D), CBR1 (E) and GSTP1 (F) in mouse livers after administering isoquercitrin and heating samples at different temperatures, respectively. Fit curves with nonlinear regression obtained with GraphPad Prism Biostatistics Software are shown.

antioxidant, anti-inflammatory, anti-hypertensive, and anti-depressant effects of this plant have been explored.[16] Many flavonol glycosides have been isolated from AV, and isoquercitrin is one of the principal flavonol glycosides in AV leaves. Isoquercitrin reduces ROS levels and inhibits lipid peroxidation and adipocyte differentiation.[27,28] In the present study, to determine whether this plant has an anti-obesity effect and which compounds are the main active components, we used separation and purification techniques of natural product chemistry. Obese mice induced with a HFD were used in researching the active fractions, active single molecules, and anti-obesity effect. Changes in the body weight gain, food intake, water consumption, liver weight and blood parameters of obese mice after treatment with the AV aqueous extract and isoquercitrin are shown in Fig. 1–3 and ESI Tables 1 and 2.† The results indicated that the AV aqueous extract had a significant anti-obesity effect and isoquercitrin is one of the main active compounds. Furthermore, in contrast to anti-obesity agents,[23] the AV aqueous extract and isoquercitrin not only reduced body weight and fat accumulation but also limited appetite and thirst in obese mice through the natural satiety process, suggesting their bidirectional effects.

To understand the mechanism of action of this plant, we used isoquercitrin as a small-molecule probe. AMPK is a highly conserved enzyme that regulates cellular energy homeostasis mainly by promoting glucose and fatty acid uptake. It is an upstream kinase of SREBP-1c and phosphorylates and inhibits its activity by preventing its proteolytic degradation and nuclear translocation.[13] SREBP-1c, an important transcription factor controlling lipolysis and fatty acid synthesis, is a hallmark of hepatic lipid metabolism.[12] It regulates the expression of central lipogenic enzymes (FAS and SCD1) and fatty acid importer protein (CD36) as downstream targets. Fatty liver in obesity is directly associated with increased SREBP-1c expression. In addition, isoquercitrin stimulates the AMPK signaling pathway in rat H4IIE cells, prevents lipid metabolic disorder *in vitro*,[24] and prevents NAFLD by modulating AMPK and TGF-β signaling *in vivo*.[29] Therefore, to obtain insights into the anti-obesity effects of isoquercitrin, we focused on the AMPK/SREBP-1 signaling pathway. The results of AMPK and SREBP-1c inhibitor experiments and gene expression-related adipogenesis (Fig. 3C, 4 and 5 and ESI Table 3†) indicated that the AMPK/SREBP-1c signaling pathway contributes to the anti-obesity effect of isoquercitrin.

Given the link between glucose metabolism and fat metabolism,[30] excess glucose uptake increases the rate of fat synthesis in the liver,[30] and glycolysis and tricarboxylic acid cycle play important roles.[31] In the present study, we found that isoquercitrin is involved not only in fatty acid metabolism but also in glucose metabolism. Therefore, we investigated the effects of isoquercitrin on glucose uptake in the intestines of mice. Changes in blood glucose concentration after the administration of isoquercitrin and the genes expression of *GLUT* shown in Fig. 6 revealed that isoquercitrin prevented glucose uptake in the intestine by regulating GLUT gene expression. Furthermore, we investigated the effect of isoquercitrin on glucose metabolism by measuring the extracellular acidification rate. Significant reduction in the extracellular acidification rate shown in Fig. 7 indicated that isoquercitrin inhibits the glycolytic pathway in HeLa cells. To determine which protein is targeted by this compound, we performed 2DE-CETSA analysis for the pre-identification of proteins. The results in Fig. 8 revealed that C-1-tetrahydrofolate synthase in the cytoplasm, protein-glutamine gamma-glutamyltrasferase E, aldo-keto

reductase family 1 member B1, proteasome activator complex subunit 3, citrate synthase in the mitochondria, and glutathione *S*-transferase P may be the potential target proteins of isoquercitrin in HeLa cells. To determine whether these proteins are the potential target proteins in HeLa cells *in vitro* and *in vivo* in mice, we used CETSA and western blotting to confirm them in HeLa cells and mouse livers. The results in Fig. 9 suggested that isoquercitrin targets multiple proteins, such as C-1-tetrahydrofolate synthase, carbonyl reductase, and glutathione *S*-transferase P to produce an anti-obesity effect.

C-1-Tetrahydrofolate synthase is an important component of the folic acid metabolic pathway and affects lipid synthesis given the association between C-1-tetrahydrofolate synthase and fatty acid synthesis through an NDAPH-dependent mechanism and thus plays an important role in lipid synthesis metabolism.[32] Carbonyl reductases are short-chain dehydrogenases or reductases which are NADPH dependent and mostly monomeric cytosolic enzymes with extensive substrate specificity for many endogenous and xenobiotic carbonyl compounds. They catalyze the reduction of endogenous steroids and other aliphatic aldehydes and ketones.[33] Glutathione plays an important role in protecting hepatocytes against toxic injury in the liver. It is the most important antioxidant in the mammalian liver. Glutathione transferases catalyze glutathione conjugation to electrophilic compounds primarily produced from exogenous xenobiotics and endogenous substances. The glutathione conjugation reaction is the key step of the mercapturic acid pathway, which is one of the most important detoxification processes.[34] These results revealed that isoquercitrin cuts off the supply of essential substances for fat synthesis by targeting these enzymes.

In conclusion, an HFD-induced obese mouse model was used in investigating the anti-obesity effect of the AV aqueous extract and isoquercitrin and its mechanism of action. Both ameliorated the symptoms of obese mice by inhibiting the AMPK/SREBP-1c/FAS/CD36 signaling pathway, glucose uptake, and glycolysis flux. Moreover, we identified that C-1-tetrahydrofolate synthase, carbonyl reductase, and glutathione *S*-transferase P protein are potential target proteins of isoquercitrin, while further research is required to identify their relationship. Isoquercitrin elicited the same hypoglycemic effect as the first-line drugs for diabetes in obese mice. Therefore, isoquercitrin might be developed as a drug or an adjuvant to prevent or treat obesity.

4. Materials and methods

4.1. General

Column chromatography was carried out using a reversed phase (octadecylsilyl, ODS) open column (Cosmosil 75 C_{18} OPN, Nacalai Tesque, Japan). Thin-layer chromatography (TLC) analysis of samples was performed with precoated silica gel plates (0.25 mm) and RP-18 (0.25 mm) plates. An Agilent 6224A accurate mass time-of-flight LC/MS system (Agilent Technologies, Santa Clara, California, USA) was used for high-resolution electrospray ionization mass spectrometry. The NMR spectrum was measured using a Bruker AV III-500 spectrometer (Bruker, Billerica, MA, USA). NMR chemical shifts in ppm were set as the reference for methanol at δ_H (3.30) and δ_C (49.0).

4.2. Preparation of the aqueous extract of AV, extraction of *A. venetum* L. and isolation and structural elucidation of isoquercitrin

Dried AV leaves were bought from Korla, Xingjiang Mongolian Autonomous Prefecture in Bayingolin, China. Approximately 90 g of the dried leaves were soaked in 300 mL of water and boiled for 5 min. The liquid part was filtered with filter paper, the filtrate was kept, and the residue was soaked in 250 mL of water, boiled for 5 min, and filtered. Finally, the obtained residue was soaked in 250 mL of water, boiled for 5 min, and filtered. This process was repeated three times. The eluents were combined and concentrated with a rotary evaporator. Isoquercitrin was isolated by separating the obtained crude water extract (5.937 g) with an ODS open column and eluted with MeOH/H_2O (20 : 80, 25 : 75, 30 : 70, 35 : 65, 50 : 50, 70 : 30, 90 : 10, and 100 : 0). Five fractions were obtained. Next, 800 mg of a fraction containing isoquercitrin was further separated with an ODS open column and eluted successively with MeOH/H_2O in ratios of 10 : 90, 11 : 89, 12 : 88, 13 : 87, 15 : 85, 20 : 80, and 100 : 0. Another five fractions were obtained, where 144 mg of isoquercitrin was a component of a separated fraction (3) as a pure compound. The chemical structure of isoquercitrin was identified by comparing the spectroscopic results in the literature,[35] ^{1}H NMR (500 MHz, CD_3OD, ESI Fig. 3†): δ_H = 7.71 (1H, d, J = 2.3 Hz, H-2′), 7.59 (1H, dd, J = 8.4, 2.1 Hz, H-6′), 6.87 (1H, d, J = 8.4 Hz, H-5′), 6.38 (1H, d, J = 2.1 Hz, H-8), 6.19 (1H, d, J = 2.1 Hz, H-6), 5.25 (1H, d, J = 7.6 Hz, H-1″), 3.72 (1H, dd, J = 11.9, 2.5 Hz, H-6″), 3.58 (1H, dd, J = 12.0, 5.5 Hz, H-6″), 3.48 (1H, m, H-3″), 3.42 (1H, m, H-2″), 3.35 (1H, m, H-4″), 3.21 (1H, m, H-5″); ^{13}C NMR (125 MHz, CD_3OD): δ = 179.5, 165.9, 163.0, 158.9, 158.4, 149.8, 145.9, 135.6, 123.2, 123.1, 117.6, 115.9, 105.7, 104.3, 99.8, 94.7, 78.4, 78.1, 75.7, 71.2 and 62.5; HR-ESI-TF-MS, m/z 465.1022, calculated for $C_{21}H_{21}O_{12}(M + H)^+$ 465.1028. The chemical structure of isoquercitrin is shown in Fig. 1A.

4.3. Animal experimental design

Four or five week-old ICR male mice from Zhejiang Academy of Medical Sciences, Hangzhou, China, were used for animal experiments (animal production permit number: SCXK (Zhe) 2019-0002). The animals were kept in a clean facility with a 24 h light and dark cycle, and the room temperature was maintained at 23 ± 1 °C for one week for adaptation. The animals were fed with either a normal diet (ND) or HFD according to the experimental design. The composition of the HFD was 24.2% crude protein, 42.1% carbohydrate, and 25.4% fat (Biotech HD Co. Ltd, Beijing, China). All the animal experiments were performed according to the guidelines of the National Institutes of Health for the care and use of laboratory animals. Standard experimental protocols were used according

to the requirements of the committee on the ethics of animal experiments of Zhejiang University (animal use permit number: SYXK (Zhe) 2018-0016, permit number: ZJU20200090). Oral administration was performed, and MilliQ water as a vehicle was used. In the first trial of the AV aqueous extract, 50 male mice aged 6 weeks were divided into five groups. The ND control group received water and ND, whereas the other groups received water and the HFD *ad libitum*, respectively. Three treatment groups received the AV aqueous extract at doses of 5, 50, and 200 mg per kg body weight per day for 5 weeks. However, in the isoquercitrin trial, 56 male ICR mice at 5 weeks were divided into seven groups (ND control, HFD control, HFD + 140 mg kg^{-1} metformin as the positive control group, HFD + 5 mg kg^{-1} AV aqueous extract, and HFD plus 0.1, HFD plus 0.5, and HFD plus 5 mg kg^{-1} isoquercitrin groups). Each group had eight mice. Body weight, food intake, and water consumption were recorded every week. The blood samples of mice were collected from the orbital venous sinus with a capillary tube, and the mice were sacrificed by neck dislocation at the end of the animal experiments. The heart, kidney, liver, spleen, pancreas, and white adipose tissues were collected as samples and stored at −30 °C for further analysis. All the experiments were repeated two times.

For the identification of the potential target protein of isoquercitrin in mice *in vivo*, six ICR mice at 6 weeks were divided into control and treatment groups. The mice of both groups received MilliQ water and isoquercitrin at a dose of 5 mg kg^{-1} day^{-1}, respectively. After the compound was applied for 1 week, the livers of mice were collected for the cellular thermal shift assay and western blotting analysis.

4.4. Measurement of the biochemical indexes of blood

At the end of the experiments, plasma samples were sent to Hangzhou Houai Biotechnology Co., Ltd (Hangzhou, Zhejiang Province, China) to detect the levels of alanine aminotransferase (ALT), aspartate aminotransferase (AST), triglycerides (TG), total cholesterol (TC), high density lipoprotein (HDL), low density lipoprotein (LDL), and glucose in the plasma with a Bio-Chemical Analyzer (COBAS 8000; Roche, Basel, Switzerland) and assay kits (Roche, Basel, Switzerland) successively.

4.5. SREBP-1c and AMPK inhibition experiments of mice *in vivo*

For the SREBP-1c inhibition experiment, 40 male ICR mice at 6 weeks were divided into four groups. The mice of the ND and HFD control groups received water, ND, or HFD *ad libitum*. One treatment group received 5 mg kg^{-1} day^{-1} isoquercitrin. For the other groups, 5 mg kg^{-1} isoquercitrin was administered, or the SREBP-1c specific inhibitor was intraperitoneally injected at a dose of 2 mg kg^{-1} for 2 weeks. Meanwhile, the mice of the treatment groups received the HFD and water *ad libitum*. In the AMPK inhibition experiment, a similar study design was used except for the fourth group, which received isoquercitrin (5 mg kg^{-1} day^{-1}) and the AMPK-specific inhibitor at a dose of 4 mg kg^{-1} through intraperitoneal injection. At the end of the experiment, the trial mice were sacrificed, and the organs were collected for further analysis.

4.6. Measurement of hepatic TG and TC levels

Approximately 200 mg of each liver sample obtained in the end of the animal experiment was homogenized in physiological saline at a 1 : 9 volume ratio. The homogenate was centrifuged, and the TG and TC contents in the supernatant were measured with TG and TC assay kits (Beijing Beihuakangtai Company, Beijing, China) according to the manufacturer's protocols, respectively.

4.7. Glucose uptake inhibition analysis

The experiment was performed as described in another report.[36] First, male ICR mice at 5 weeks were divided into two groups and were fasted for 24 h. The mice were orally administered with isoquercitrin *via* the co-administration or pretreatment method. In the co-administration experiment, 12.5 mg of D-glucose with or without isoquercitrin dissolved in distilled water was administered to mice *via* oral gavage. In the pretreatment method, isoquercitrin (6.25 μM) and D-glucose (12.5 mg) were dissolved in distilled water, respectively. The D-Glucose solution was orally administered after the administration of isoquercitrin and the vehicle for 10 min. Subsequently, the blood glucose levels of mice were measured at 5, 15, 30, 60, 90 and 120 min with a glucometer (Andon Health, Tianjin, China) by using the blood collected from the tip of the tail vein.

4.8. Real-time polymerase chain reaction (RT-PCR)

The collected and weighed liver and epididymal fat tissues were immediately kept at −30 °C until further experimentation. The frozen samples were subjected to RNA extraction, quantification and cDNA synthesis using a method described in previous studies.[37] Approximately 50 mg of liver tissue of each mouse was taken to extract RNA by using the Trizol reagent (Invitrogen, California, USA). Reverse transcription was carried out using approximately 2.5 μg of total RNA from each sample. A HiFi-MMLV cDNA kit (Fermentas, Shenzhen, China) was used. Real-time PCR analysis was performed using a CFX96 Touch (Bio-Rad, Hercules, CA, USA) and SYBR Premix EX Taq™ (Takara, Otsu, Japan). The mouse primers of SREBP-1c, SCD-1, FAS, CD-36, GLUT1, GLUT2, GLUT4, and 18S RNA employed for PCR analysis are revealed in ESI Table 4.† The conditions for cDNA amplification were as follows: 95 °C for 30 s, followed by 40 cycles for 5 s at 95 °C, and 34 s at 60 °C. After normalizing the data to 18S RNA levels, the $2^{-\Delta\Delta Ct}$ formula was used to estimate the relative and trancripted mRNA levels. Average values were considered after running the samples in triplicate.

4.9. Target protein investigation for isoquercitrin by 2D gel electrophoresis based proteome-wide CETSA

2DE-CETSA was performed according to a method previously described in detail.[38] Briefly, HeLa cell lysates (2 mg mL^{-1}

protein) with compounds (50 μM) or DMSO were heated at an indicated temperature for 5 min. The supernatants obtained through the centrifugation of the resultant solutions were analyzed by 2-D DIGE. The log ratios of the test compound-treated sample to the DMSO-treated sample in each spot signal were calculated and analyzed by drawing melting curves. Afterward, some spots with thermo-stability change were selected and identified through LC-MS/MS.

4.10. Cellular thermal shift assay

To confirm the target proteins at cell and animal levels, the protein samples of HeLa cells and livers of animals were prepared as per the following step. CETSA was performed as described in other reports.[39] At first, HeLa cells, which were purchased from Procell Life Science & Technology Co., Ltd (Wuhan, China), were cultured in RPMI-1640 medium containing 1% penicillin–streptomycin solution and 10% fetal bovine serum (CellMax Cell Technology Co., Ltd Beijing, China) for five days after resuscitation. When the cells reached 80% coverage, approximately 1×10^6 HeLa cells were seeded in each 60 mm culture dish containing 5 mL of RPMI-1640 medium, and incubated in 5% CO_2 at 37 °C for 24 h. On the next day, the medium in the dishes was replaced with 5 mL serum-free RPMI-1640 medium containing 0.5% DMSO and isoquercitrin at 50 μM and the cells in the dishes were continually incubated for 2 h, respectively. After that, the cells were then washed thrice with PBS and lysed with RAPI lysis buffer (CoWin Biotech, Beijing, China) containing 1% protease inhibitor cocktail (CoWin Biotech, Beijing, China), and incubated on ice for 20 min. The cell lysates were centrifuged, and the supernatant was removed for the cellular thermal shift assay. HeLa cell lysates (2 μg μL^{-1} protein) were heated at an indicated temperature for 5 min. The supernatants were obtained as the samples for western blot analysis after centrifugation. In addition, the fresh liver samples of mice in isoquercitrin and control groups were obtained and lysed with PBS buffer. The liver lysates (100 μg) of the control and treatment groups were heated at an indicated temperature for 5 min. The supernatants obtained through the centrifugation of the resultant solutions were analyzed with western blot. Western blot analysis was used to detect changes in a target protein with specific antibodies [anti-MTHFD1 and anti-PSME3 (#ab103698 and #ab157157, Abcam Trading Company Ltd, Shanghai, China) for C-1-tetrahydrofolate synthase and proteasome activator complex subunit 3, and anti-CRB1 and anti-GSTP1 (#bs-8632R and #bs-23151R, Bioss Antibodies Biotechnology Co., Ltd, Beijing, China) for carbonyl reductase and glutathione *S*-transferase P]. The secondary antibodies horseradish peroxidase-linked goat anti-rabbit (#CW0103, CoWin Biotech, Beijing, China) for MTHFD1, GSTP1, CBR1, and PSME3, and goat anti-mouse IgGs (#CW0102, CoWin Biotech, Beijing, China) for β-actin (#CW0096M, CoWin Biotech, Beijing, China) were used in the present study. The antigens were detected using an ECL western blot kit, whereas the protein bands were analyzed using ImageJ (Version 1.42q, National Institutes of Health, Rockville, MD, United States).

4.11. Oxygen consumption rates and external cellular acidification rate assay

Oxygen consumption rates (OCRs) and external cellular acidification rates (ECARs) were measured with an Xfe96 extracellular flux analyzer (Agilent), as described in another report.[40] Briefly, HeLa cells of third passage were seeded at a density of 10 000 cells per well of an XFe96 cell culture microplate and incubated for 24 h. Before the assay, the cells were equilibrated for 1 h in a non-CO_2 incubator with RPMI 1640 (R1383, Sigma) supplemented with 1% FCS and 0 mM glucose (for glucose stimulation experiments) or 10 mM glucose. Injector ports were used to deliver the reagents, including AA (the combined treatment of 30 μM A769662 and 2 mM AICAR), and isoquercitrin at doses of 1, 3, and 10 μg mL^{-1}. Data were analyzed using Wave (version 2.6; Agilent).

4.12. Statistical analysis

GraphPad Prism Biostatistics (GraphPad Prism, San Diego, USA) was used to perform statistical analysis. Significant differences among animal experiments were determined using one-way ANOVA, followed by Tukey's multiple comparison test. Data were represented as means ± SEM and $^*p < 0.05$ or $^{\#}p < 0.05$ indicated statistical significance.

Author contributions

Methodology and writing – original draft: Majid Manzoor; data curation: Majid Manzoor, Makoto Muroi, Naoko Ogawa, Hiroki Kobayashi, Haruna Nishimura, Danni Chen, Opeyemi B. Fasina and Jianyu Wang; conceptualization: Lan Xiang and Jianhua Qi; supervision and project administration: Lan Xiang, Jianhua Qi, Hiroyuki Osada, and Minoru Yoshida; and writing – review & editing: Lan Xiang, Jianhua Qi, Hiroyuki Osada and Minoru Yoshida. All authors agreed to their individual contributions and the final manuscript.

Abbreviations

AMPK	Adenosine 5′-monophosphate-activated protein kinase
ALT	Alanine aminotransferase
AST	Aspartate aminotransferase
CD36	Cluster of differentiation 36
CETSA	Cellular thermal shift assay
DMSO	Dimethyl sulfoxide
ECARs	External cellular acidification rates
FAS	Fatty acid synthase
GLUT	Glucose transporter
HFD	High fat diet
HDL	High density lipoprotein
ICR	Institute of Cancer Research
LDL	Low density lipoprotein
ND	Normal diet
OCRs	Oxygen consumption rates

SREBP	Sterol regulatory-element binding protein
RT-PCR	Real-time polymerase chain reaction
SCD-1	Stearoyl-CoA desaturase-1
TG	Triglycerides
TC	Total cholesterol
2-D DIGE	Two-dimensional fluorescence difference gel electrophoresis

Conflicts of interest

All authors declare that there are no competing financial interests.

Acknowledgements

This work was financially supported by the National Key R&D Program of China (Grant No. 2019YFE0100700) and the National Natural Science Foundation of China (Grant No. 21877098, 22177102). This work was also supported in part by Grants-in-Aid for Scientific Research (Grant Numbers 19H05640 and 18H05503 to M. Y.) from the Ministry of Education, Culture, Sports, Science and Technology of Japan, and was inspired by the Asian Chemical Biology Initiative, JSPS.

References

1 W.H. Organization, Obesity and overweight. Fact Sheet. June 2016, Retrieved from [Jan 2017], 2017.
2 G.O. Collaborators, Health effects of overweight and obesity in 195 countries over 25 years, *N. Engl. J. Med.*, 2017, **377**, 13–27.
3 J.-P. Després and I. Lemieux, Abdominal obesity and metabolic syndrome, *Nature*, 2006, **444**, 881–887.
4 C. Jin, J. Henao-Mejia and R. A. Flavell, Innate immune receptors: key regulators of metabolic disease progression, *Cell Metab.*, 2013, **17**(6), 873–882.
5 M. E. Bocarsly, M. Fasolino, G. A. Kane, E. A. LaMarca, G. W. Kirschen, I. N. Karatsoreos, B. S. McEwen and E. Gould, Obesity diminishes synaptic markers, alters microglial morphology, and impairs cognitive function, *Proc. Natl. Acad. Sci. U. S. A.*, 2015, **112**, 15731–15736.
6 I. J. Onakpoya, C. J. Heneghan and J. K. Aronson, Post-marketing withdrawal of anti-obesity medicinal products because of adverse drug reactions: a systematic review, *BMC Med.*, 2016, **14**, 191.
7 D. Garcia and R. J. Shaw, AMPK: mechanisms of cellular energy sensing and restoration of metabolic balance, *Mol. Cell*, 2017, **66**, 789–800.
8 R. Rafaeloff-Phail, L. Ding, L. Conner, W.-K. Yeh, D. McClure, H. Guo, K. Emerson and H. Brooks, Biochemical regulation of mammalian AMP-activated protein kinase activity by NAD and NADH, *J. Biol. Chem.*, 2004, **279**, 52934–52939.
9 L. G. Fryer, A. Parbu-Patel and D. Carling, The anti-diabetic drugs rosiglitazone and metformin stimulate AMP-activated protein kinase through distinct signaling pathways, *J. Biol. Chem.*, 2002, **277**, 25226–25232.
10 K. A. Coughlan, R. J. Valentine, N. B. Ruderman and A. K. Saha, AMPK activation: a therapeutic target for type 2 diabetes?, *Diabetes, Metab. Syndr. Obes.: Targets Ther.*, 2014, **7**, 241.
11 J. B. Kim and B. M. Spiegelman, ADD1/SREBP1 promotes adipocyte differentiation and gene expression linked to fatty acid metabolism, *Genes Dev.*, 1996, **10**, 1096–1107.
12 M. S. Brown and J. L. Goldstein, The SREBP pathway: regulation of cholesterol metabolism by proteolysis of a membrane-bound transcription factor, *Cell*, 1997, **89**, 331–340.
13 Y. Li, S. Xu, M. M. Mihaylova, B. Zheng, X. Hou, B. Jiang, O. Park, Z. Luo, E. Lefai and J. Y.-J. Shyy, AMPK phosphorylates and inhibits SREBP activity to attenuate hepatic steatosis and atherosclerosis in diet-induced insulin-resistant mice, *Cell Metab.*, 2011, **13**, 376–388.
14 L. Wu, L. Zhang, B. Li, H. Jiang, Y. Duan, Z. Xie, L. Shuai, J. Li and J. Li, AMP-activated protein kinase (AMPK) regulates energy metabolism through modulating thermogenesis in adipose tissue, *Front. Physiol.*, 2018, **9**, 122.
15 H. Liu, J. Wang, M. Liu, H. Zhao, S. Yaqoob, M. Zheng, D. Cai and J. Liu, Antiobesity effects of ginsenoside Rg1 on 3T3-L1 preadipocytes and high fat diet-induced obese mice mediated by AMPK, *Nutrients*, 2018, **10**, 830.
16 W. Xie, X. Zhang, T. Wang and J. Hu, Botany, Traditional uses, phytochemistry and pharmacology of Apocynum venetum L.(Luobuma): A review, *J. Ethnopharmacol.*, 2012, **141**, 1–8.
17 Y. Zhang, C. Liu, Z. Zhang, J. Wang, G. Wu and S. Li, Comprehensive separation and identification of chemical constituents from Apocynum venetum leaves by high-performance counter-current chromatography and high performance liquid chromatography coupled with mass spectrometry, *J. Chromatogr. B: Anal. Technol. Biomed. Life Sci.*, 2010, **878**, 3149–3155.
18 Q. Xiong, W. Fan, Y. Tezuka, I. K. Adnyana, P. Stampoulis, M. Hattori, T. Namba and S. Kadota, Hepatoprotective effect of Apocynum venetum and its active constituents, *Planta Med.*, 2000, **66**, 127–133.
19 O. Grundmann, J.-I. Nakajima, S. Seo and V. Butterweck, Anti-anxiety effects of Apocynum venetum L. in the elevated plus maze test, *J. Ethnopharmacol.*, 2007, **110**, 406–411.
20 B.-H. Kim, J. S. Choi, E. H. Yi, J.-K. Lee, C. Won, S.-K. Ye and M.-H. Kim, Relative antioxidant activities of quercetin and its structurally related substances and their effects on NF-κB/CRE/AP-1 signaling in murine macrophages, *Mol. Cells*, 2013, **35**, 410–420.
21 S. Panda and A. Kar, Antidiabetic and antioxidative effects of Annona squamosa leaves are possibly mediated through quercetin–3–O–glucoside, *Biofactors*, 2007, **31**, 201–210.
22 K. Ohguchi, C. Nakajima, M. Oyama, M. Iinuma, T. Itoh, Y. Akao, Y. Nozawa and M. Ito, Inhibitory effects of flavo-

noid glycosides isolated from the peel of Japanese persimmon (Diospyros kaki 'Fuyu') on melanin biosynthesis, *Biol. Pharm. Bull.*, 2010, **33**, 122–124.

23 J. Erdmann, F. Lippl, G. Klose and V. Schusdziarra, Cholesterol lowering effect of dietary weight loss and orlistat treatment–efficacy and limitations, *Aliment. Pharmacol. Ther.*, 2004, **19**, 1173–1179.

24 J. Zhou, H. Yoshitomi, T. Liu, B. Zhou, W. Sun, L. Qin, X. Guo, L. Huang, L. Wu and M. Gao, Isoquercitrin activates the AMP–activated protein kinase (AMPK) signal pathway in rat H4IIE cells, *BMC Complementary Altern. Med.*, 2014, **14**, 1–10.

25 R. San-Cristobal, S. Navas-Carretero, M.Á Martínez-González, J. M. Ordovas and J. A. Martínez, Contribution of macronutrients to obesity: implications for precision nutrition, *Nat. Rev. Endocrinol.*, 2020, **16**, 1–16.

26 L. Xiang, Q. Wu, L. Cheng, K. Sun, J. Li, M. Yoshida and J. Qi, Leptin and adiponectin signaling pathways are involved in the antiobesity effects of peanut skin extract, *Oxid. Med. Cell. Longevity.*, 2019, **2019**, 2935315.

27 R. Li, C. Yuan, C. Dong, S. Shuang and M. M. Choi, In vivo antioxidative effect of isoquercitrin on cadmium-induced oxidative damage to mouse liver and kidney, *Naunyn Schmiedebergs Arch. Pharmacol.*, 2011, **383**, 437–445.

28 S. H. Lee, B. Kim, M. J. Oh, J. Yoon, H. Y. Kim, K. J. Lee, J. D. Lee and K. Y. Choi, Persicaria hydropiper (L.) spach and its flavonoid components, isoquercitrin and isorhamnetin, activate the Wnt/β–catenin pathway and inhibit adipocyte differentiation of 3T3–L1 cells, *Phytother. Res.*, 2011, **25**, 1629–1635.

29 G. Qin, J. Ma, Q. Huang, H. Yin, J. Han, M. Li, Y. Deng, B. Wang, W. Hassan and J. Shang, Isoquercetin improves hepatic lipid accumulation by activating AMPK pathway and suppressing TGF-β signaling on an HFD-induced nonalcoholic fatty liver disease rat model, *Int. J. Mol. Sci.*, 2018, **19**, 4126.

30 L. P. Bechmann, R. A. Hannivoort, G. Gerken, G. S. Hotamisligil, M. Trauner and A. Canbay, The interaction of hepatic lipid and glucose metabolism in liver diseases, *J. Hepatol.*, 2012, **56**, 952–964.

31 L. Rui, Energy metabolism in the liver, *Compr. Physiol.*, 2011, **4**, 177–197.

32 H. Wang, Q. Wang, C. Zhang, H. Chen, W. Lu, Z. Gu, J. Zhao, H. Zhang, Y. Q. Chen and W. Chen, The role of MTHFDL in mediating intracellular lipogenesis in oleaginous Mortierella alpina, *Microbiology*, 2020, **166**, 617–623.

33 G. L. Forrest and B. Gonzalez, Carbonyl reductase, *Chem.-Biol. Interact.*, 2000, **129**, 21–40.

34 J. R. Bertino, *Encyclopedia of Cancer. Set*, Academic Press [Imprint], 2002.

35 I. Atay, H. Kirmizibekmez, A. C. GÖREN and E. YEŞİLADA, Secondary metabolites from Sambucus ebulus, *Turk. J. Chem.*, 2015, **39**, 34–41.

36 T. Furuta, Y. Mizukami, L. Asano, K. Kotake, S. Ziegler, H. Yoshida, M. Watanabe, S.-i. Sato, H. Waldmann and M. Nishikawa, Nutrient-Based Chemical Library as a Source of Energy Metabolism Modulators, *ACS Chem. Biol.*, 2019, **14**, 1860–1865.

37 L. Xiang, J. Li, Q. Wang, R. Tang and J. Qi, Leptin gene transfer improves symptoms of type 2 diabetic mice by regulating leptin signaling pathway and insulin resistance of peripheral tissues, *Hum. Gene Ther.*, 2018, **29**, 68–76.

38 I. Nagasawa, M. Muroi, M. Kawatani, T. Ohishi, S.-i. Ohba, M. Kawada and H. Osada, Identification of a small compound targeting PKM2-regulated signaling using 2D gel electrophoresis-based proteome-wide CETSA, *Cell Chem. Biol.*, 2020, **27**, 186–196.

39 J. Li, K. Sun, M. Muroi, L. Gao, Y. T. Chang, H. Osada, L. Xiang and J. Qi, Cucurbitacin B induces neurogenesis in PC12 cells and protects memory in APP/PS1 mice, *J. Cell. Mol. Med.*, 2019, **23**, 6283–6294.

40 H. Kobayashi, H. Hatakeyama, H. Nishimura, M. Yokota, S. Suzuki, Y. Tomabechi, M. Shirouzu, H. Osada, M. Mimaki, Y.-i. Goto and M. Yoshida, Chemical reversal of abnormalities in cells carrying mitochondrial DNA mutations, *Nat. Chem. Biol.*, 2021, **17**, 335–343.